Monthly Notices
of the
ROYAL ASTRONOMICAL SOCIETY

Mon. Not. R. Astron. Soc. **412,** 1047–1058 (2011) doi:10.1111/j.1365-2966.2010.17966.x

A carbon-enhanced metal-poor damped Lyα system: probing gas from Population III nucleosynthesis?⋆

Ryan Cooke,[1]† Max Pettini,[1] Charles C. Steidel,[2] Gwen C. Rudie[2] and Regina A. Jorgenson[1]

[1] *Institute of Astronomy, Madingley Road, Cambridge CB3 0HA*
[2] *California Institute of Technology, MS 249-17, Pasadena, CA 91125, USA*

Accepted 2010 November 1. Received 2010 November 1; in original form 2010 July 29

ABSTRACT

We present high-resolution observations of an extremely metal-poor damped Lyα system (DLA), at $z_{\rm abs} = 2.340\,0972$ in the spectrum of the QSO J0035−0918, exhibiting an abundance pattern consistent with model predictions for the supernova yields of Population III stars. Specifically, this DLA has [Fe/H] $\simeq -3$, shows a clear 'odd–even' effect, and is C-rich with [C/Fe] $= +1.53$, a factor of ∼20 greater than reported in any other DLA. In analogy to the carbon-enhanced metal-poor stars in the Galactic halo (with [C/Fe] $> +1.0$), this is the first known case of a carbon-enhanced DLA. We determine an upper limit to the mass of ^{12}C, $M(^{12}{\rm C}) \leq 200\,{\rm M}_{\odot}$, which depends on the unknown gas density n(H); if $n({\rm H}) > 1\,{\rm cm}^{-3}$ (which is quite likely for this DLA given its low velocity dispersion), then $M(^{12}{\rm C}) \leq 2\,{\rm M}_{\odot}$, consistent with pollution by only a few prior supernovae. We speculate that DLAs such as the one discovered here may represent the 'missing link' between the yields of Population III stars and their later incorporation in the class of carbon-enhanced metal-poor stars which show no enhancement of neutron-capture elements (CEMP-no stars).

Key words: stars: carbon – stars: Population III – galaxies: abundances – galaxies: evolution – quasars: absorption lines – quasars: individual: J0035−0918.

1 INTRODUCTION

Damped Lyα systems (DLAs) are the neutral gas reservoirs at high redshift that have, by definition, neutral hydrogen column densities in excess of $10^{20.3}$ atoms cm^{-2} (see Wolfe, Gawiser & Prochaska 2005 for a review). At these high column densities the gas is self-shielded (e.g. Vladilo et al. 2001), resulting in a simple ionization structure which facilitates the derivation of element abundances. Moreover, the abundances thus derived are independent of the geometrical configuration and thermodynamical state of the gas, and of most other factors which complicate the analysis of stellar spectra (e.g. Asplund 2005). The largest uncertainties in DLA abundance studies are due to the effects of line saturation and dust depletion (for some elements), although the latter of these concerns is found to be minimal when the metallicity of the DLA is below $\sim 1/100\,{\rm Z}_{\odot}$ (Pettini et al. 1997; Prochaska & Wolfe 2002; Akerman et al. 2005).

In recent years, these very metal poor (VMP) DLAs, with metallicities [Fe/H][1] < -2, have attracted an increasing amount of interest because of their potential for probing gas which may still bear the chemical imprint of the first few generations of stars to have formed in the Universe (e.g. Erni et al. 2006). They are thus an extremely valuable complement, at high redshifts, to local studies of the oldest and most metal-poor stars in the Galactic halo.

The VMP DLA regime was largely unexplored until very recently, when it became possible to identify candidate metal-poor DLAs in Sloan Digital Sky Survey (SDSS) quasars, and then measure their chemical composition with high-resolution follow-up spectroscopy. The first high spectral resolution ($R \gtrsim 30\,000$, full width at half-maximum, FWHM $\lesssim 10\,{\rm km\,s}^{-1}$) sample of VMP DLAs was compiled by Pettini et al. (2008), whose main goal was to compare the relative abundances of C, N and O with the trends observed in VMP halo stars in our Galaxy. More recently, Penprase et al. (2010) have presented medium resolution (FWHM ∼ $60\,{\rm km\,s}^{-1}$) spectroscopy of a sample of 27 VMP DLAs to explore the general properties of DLAs in the VMP regime. However, as Penprase et al. acknowledge themselves, there are difficulties with

⋆Based on data obtained at the W. M. Keck Observatory, which is operated as a scientific partnership among the California Institute of Technology, the University of California and NASA, and was made possible by the generous financial support of the W. M. Keck Foundation.

†E-mail: rcooke@ast.cam.ac.uk

[1] We adopt the standard notation: $[{\rm A/B}] \equiv \log(N_{\rm A}/N_{\rm B}) - \log(N_{\rm A}/N_{\rm B})_{\odot}$, where $N_{\rm A,B}$ refers to the number of atoms of element A and B.

accurately measuring column densities from medium (as opposed to high) resolution data, given that most DLAs with metallicities less than 1/100 solar exhibit very low velocity dispersions, with metal linewidths less than 10 km s^{-1} (Ledoux et al. 2006; Murphy et al. 2007; Prochaska et al. 2008). Under these circumstances, line saturation can easily be overlooked.

Perhaps the most startling result from abundance studies of VMP DLAs are the near-solar values of [C/O] at low metallicity (Pettini et al. 2008), in line with the peculiar upturn in the [C/O] abundance below [O/H] $\lesssim -1.0$ in Galactic halo stars discovered by Akerman et al. (2004) and later confirmed by Fabbian et al. (2009a). Akerman et al. (2004) attributed this behaviour to an increased C yield from earlier generations of massive stars. Penprase et al. (2010) extended this work and reported a number of DLAs with supersolar [C/O] suggesting that this ratio continues to increase with decreasing [O/H]. A more recent compilation of high spectral resolution observations of VMP DLAs, however, suggests that the ratio in fact plateaus at [C/O] ~ -0.2 (Cooke R. et al., in preparation).

In contrast to the relatively new interest in VMP DLAs, studies of metal-poor Galactic halo stars have received ongoing attention for more than two decades, most recently from the dedicated HK (Beers, Preston & Shectman 1992) and Hamburg/ESO (Christlieb et al. 2001) surveys. A relevant result emerging from this work is that nearly one-quarter of all metal-poor stars with [Fe/H] < -2.0 exhibit a marked carbon enhancement, with [C/Fe] $> +1.0$ (Beers & Christlieb 2005; Lucatello et al. 2006). These are collectively known as carbon-enhanced metal-poor stars (CEMP stars), and have been subdivided into four classes based on the abundances of their neutron-capture elements: (i and ii) the CEMP-s and CEMP-r classes, with enhancements of elements produced predominantly by the *s*-process and *r*-process, respectively; (iii) the CEMP-rs class, with enhancements in both the *s*- and *r*-process elements and (iv) the CEMP-no class, which exhibits no such enhancements.

For further details of these classes, and the likely origins of their carbon enhancements, we direct the reader to Masseron et al. (2010). In short, there is reasonable evidence to suggest that CEMP-s and CEMP-rs stars are extrinsically polluted by a now extinct asymptotic giant branch (AGB) companion. The origin of the CEMP-no class, however, is not yet firmly established. Whilst several models invoking mass transfer from an AGB companion could explain the lack of neutron-capture elements (e.g. Fujimoto, Ikeda & Iben 2000; Siess, Goriely & Langer 2004), radial-velocity measurements have not yet confirmed whether CEMP-no stars are host to binary companions. Indeed, the apparent difference in the metallicity distributions between CEMP-no stars and the other CEMP classes, in the sense that CEMP-no stars are more numerous at lower metallicity, might suggest that a mechanism other than the AGB binary transfer scenario produces the C enhancement in CEMP-no stars (Aoki et al. 2007). In all likelihood, as pointed out by Masseron et al. (2010), there is a continuous link that connects *some* CEMP-no stars with CEMP-s stars, while the carbon enhancement of other CEMP-no stars may have a different origin.

Models of core-collapse supernova yields from Population III (or near metal-free) stars do entertain high C yields relative to Fe (e.g. Woosley & Weaver 1995). Population III enrichment is a particularly intriguing explanation for the origin of the carbon enhancement in some CEMP stars, since the three most Fe-poor halo stars all exhibit carbon enhancements relative to iron (Christlieb et al. 2002; Frebel et al. 2005; Norris et al. 2007). Moreover, the fraction of metal-poor stars that exhibit a carbon-enhancement *increases* with decreasing metallicity (Beers & Christlieb 2005). In this Population III enrichment scenario, the carbon enhancement in the extremely metal-poor regime reflects the initial composition of the gas from which these stars formed, rather than resulting from mass transfer from an evolved companion.

Whilst the physics behind core-collapse supernovae is poorly constrained, several parametrized models have been developed to calculate the expected yields from zero-metallicity progenitors to compare with the observations of the most Fe-poor CEMP stars, as well as the more 'normal' non-CEMP stars. The most important (and largely unknown) quantities are the degree of mixing during the supernova explosion and the amount of fallback on to the remnant black hole thereafter (Umeda & Nomoto 2003). Umeda & Nomoto (2003) parametrized both quantities, then suitably selected the appropriate values that reproduce the observed stellar abundance patterns. Heger & Woosley (2010), on the other hand, parametrize only the mixing parameter by applying a running boxcar filter over the star following the explosion. This prescription successfully reproduces the chemical composition of the extremely metal-poor (non-CEMP) halo stars from the study by Cayrel et al. (2004), as well as that of the most Fe-poor CEMP stars HE0107−5240 (Christlieb et al. 2002) and HE1327−2326 (Frebel et al. 2005). Joggerst, Woosley & Heger (2009) extended this work by mapping the 1D models by Heger & Woosley (2010) on to a 2D grid to follow Rayleigh–Taylor induced mixing after explosive nuclear burning. Whilst the Joggerst et al. (2009) models are physically motivated, they are unable to reproduce the relatively high levels of nitrogen enrichment that are observed in the most Fe-poor stars, nor are they able to produce sufficient Fe-peak elements.

These concerns are alleviated with models that include rotation (e.g. Meynet, Ekström & Maeder 2006; Hirschi 2007), since rotation induces additional mixing and mass loss in the pre-supernova phase of low-metallicity stars. The only simulations available to date that investigate the effects of both rotational and Rayleigh–Taylor mixing, as well as incorporating a realistic prescription of fallback, are those presented recently by Joggerst et al. (2010a) (see also Joggerst, Almgren & Woosley 2010b). By introducing rotation in their zero-metallicity models, Joggerst et al. (2010a) report an increased nitrogen yield, as well as an increased Fe-peak element yield; however, these models are not able to reproduce the high CNO to Fe ratios observed in the most metal-poor stars. In summary, it is still a matter of some debate whether these extremely metal-poor early Population II stars: (i) were borne out of gas which had previously been carbon-enriched by the first stars; or (ii) received a CNO top-up from a companion star and/or (iii) exhibit a degree of self-pollution from their own nucleosynthesis.

The first possibility, that at least some CEMP stars were borne out of carbon-enhanced gas, is given additional support from the discovery reported here of an extremely metal-poor DLA at $z_{\rm abs} = 2.340\,0972$ exhibiting a carbon enhancement akin to that measured in Galactic CEMP stars. No other case was known until now, given (i) the rarity of DLAs with [Fe/H] < -2, which lie in the tail of the metallicity distribution of DLAs (e.g. Pontzen et al. 2008), and (ii) the difficulty in measuring [C/H] in DLAs, where the relevant absorption lines are often saturated even in the VMP regime. We speculate that this DLA may be the 'missing link' between the first few generations of stars and some of the CEMP stars in the Galactic halo.

The paper is organized as follows. Section 2 summarizes the observations and data reduction. We analyse the absorption lines of the DLA and deduce corresponding element abundances in Section 3. In Section 4 we scrutinize potential issues that could masquerade as a carbon enhancement. After ruling out these possibilities, we discuss in Section 5 possible origins of this enhancement, and consider

the implications of our finding for models of CEMP stars. Finally, we summarize our results and draw our conclusions in Section 6.

2 OBSERVATIONS AND DATA REDUCTION

The $m_r = 18.89$, $z_{em} = 2.42$ quasar (QSO) J0035−0918 was selected for our ongoing survey for VMP DLAs (Cooke R. et al., in preparation) on the basis of its SDSS spectrum which shows a DLA at $z_{abs} \simeq 2.340$ with no apparent associated metal lines. Such cases are highly suggestive of narrow and weak metal absorption lines which are undetectable at the coarse resolution and signal-to-noise ratio (S/N) of the discovery SDSS spectra.

Follow-up observations of J0035−0918 were made with the Magellan Echellette (MagE) spectrograph (Marshall et al. 2008) on the Magellan II Clay telescope on the nights of 2008 December 30 and 31 in good conditions with 1-arcsec seeing. We took 2 × 2400 s exposures using the standard setup with 1×1 binning and a 1.0-arcsec slit giving a resolving power $R \equiv \lambda/\Delta\lambda \simeq 4100$. Standard calibrations were taken following the recommendations by Simcoe, Hennawi & Williams.[2] The data were reduced using a custom set of Interactive Data Language (IDL) routines written by G. D. Becker and described in Becker et al. (2006). The MagE spectrum confirmed the VMP DLA nature of the $z_{abs} = 2.340\,0972$ absorption system, by showing clear damping wings to the Lyα absorption line (see top panel of Fig. 1) and unusually weak associated metal lines.

Encouraged by these initial indications, we subsequently observed J0035−0918 on the night of 2009 December 9 with the High Resolution Echelle Spectrograph (HIRES; Vogt et al. 1994) on the Keck I telescope under good conditions with subarcsecond seeing, for a total integration time of 16200 s, divided into six exposures of 2700 s, resulting in an S/N near 4500 Å of S/N $\simeq$ 18. We used the 1.148-arcsec wide slit which, when uniformly illuminated, provides a nominal spectral resolution $R \equiv \lambda/\Delta\lambda = 37\,000$. From our spectra, we measure $R \simeq 41\,000$ which corresponds to a velocity FWHM = 7.3 km s^{-1}, sampled by ∼3 pixels. We employed the UV cross-disperser which covers the wavelength range 3100–6000 Å with ∼70-Å wide gaps near 4000 and 5000 Å.

The HIRES spectra were reduced with the MAKEE data reduction pipeline developed by Tom Barlow, which performs the usual steps of flat-fielding, order tracing, background subtraction and extraction of the final 1D spectrum. The data were wavelength calibrated by reference to the spectrum of a ThAr lamp, and mapped on to a vacuum heliocentric wavelength scale. The extracted spectra were merged and then normalized by dividing out the QSO continuum and emission lines, using the software package UVES_POPLER, maintained by Michael Murphy.[3] Following this step, all available metal absorption lines associated with the DLA were extracted in ±150 km s^{-1} windows around the pixel with highest optical depth. A further fine correction to the continuum was then applied if necessary.

3 PROFILE FITTING AND ABUNDANCE ANALYSIS

Table 1 lists all the metal absorption lines in the $z_{abs} = 2.340\,0972$ DLA detected in our HIRES spectrum of J0035−0918, together with a few interesting transitions which are below the detection limit of the data. For each line, we give the rest-frame wavelength and oscillator strength that we adopted for this work, as well as the measured equivalent width and associated random and systematic errors. The latter were determined by shifting the continuum by $\pm\sigma/\sqrt{n}$ (where σ is the 1σ error spectrum, and n is the number of independent resolution elements over which the equivalent width integration was carried out), and recalculating the equivalent width. For the undetected transitions, we quote the 3σ limiting rest-frame equivalent width, using as a guide the profile of the weakest absorption line, Fe II λ1608, which we detect at the 5σ confidence limit (see Table 1). Examples of metal absorption lines are reproduced in Fig. 1.

As can be appreciated from inspection of Table 1 and Fig. 1, the metal lines in this DLA are very weak and narrow, with equivalent widths $W_0 < 55$ mÅ (the strongest line being C II λ1334), and with the absorption taking place in a single velocity component with FWHM < 10 km s^{-1}. The weakness of the absorption limits our detection to the intrinsically most abundant elements of the periodic table, C, N, O, Al, Si and Fe; on the other hand, the wide wavelength coverage of the echelle spectra, which reach well into the far-UV, gives access to several transitions of differing f-values for most of these elements.

3.1 Column densities

We begin our abundance analysis by measuring the column density of neutral hydrogen. To this end, we used the MagE spectrum of the QSO, the relevant portion of which is reproduced in the top panel of Fig. 1, because at $z_{abs} = 2.340\,0972$ the damped Lyα line falls on a gap between two of the CCDs in the HIRES detector mosaic. Even at the coarser resolution of MagE (compared to HIRES), the broad damped Lyα line is fully resolved and no loss of accuracy results in the derivation of N(H I). Fitting a Voigt profile to the line, we deduced $\log[N(\mathrm{H\,I})/\mathrm{cm}^{-2}] = 20.55 \pm 0.10$; the corresponding theoretical Voigt profile is overlaid on the MagE spectrum in the top panel of Fig. 1.

In the next step, we determined the Doppler parameter of the absorbing gas, b (km s^{-1}), and the column density of the metal ions, N(X) (cm^{-2}), by fitting the corresponding line profiles with VPFIT[4], which simultaneously fits multiple Voigt profiles to several atomic transitions, returning the values of N(X) and b, together with the associated errors, that minimize the χ^2 between the data and the model. We tied the redshift and the Doppler parameter to be the same for all of the absorption lines listed in Table 1, which is justified if the neutrals and first ions are kinematically associated with the same gas (we relax this assumption later). With these constraints, VPFIT converged to a best-fitting model consisting of a single absorption component with redshift $z = 2.340\,0972 \pm 0.000\,0008$ and Doppler parameter $b = 2.36 \pm 0.08$ km s^{-1}. The corresponding column densities are listed in Table 2. Examples of the theoretical line profiles generated by VPFIT are shown superimposed on the data in Fig. 1.

The weakest feature in our data is S II λ1259. When this line is included in the VPFIT fitting procedure (see bottom right panel of Fig. 1), we derive a column density $\log N(\mathrm{S\,II})/\mathrm{cm}^{-2} = 13.08 \pm 0.10$. However, since this absorption line is only significant at the ∼4.5σ level, we conservatively consider the above value to be an upper limit to the column density of S II.

[2] see http://web.mit.edu/rsimcoe/www/MagE/mage.html

[3] UVES POPLER is available from http://astronomy.swin.edu.au/∼mmurphy/UVES_popler.

[4] VPFIT is available from http://www.ast.cam.ac.uk/∼rfc/vpfit.html.

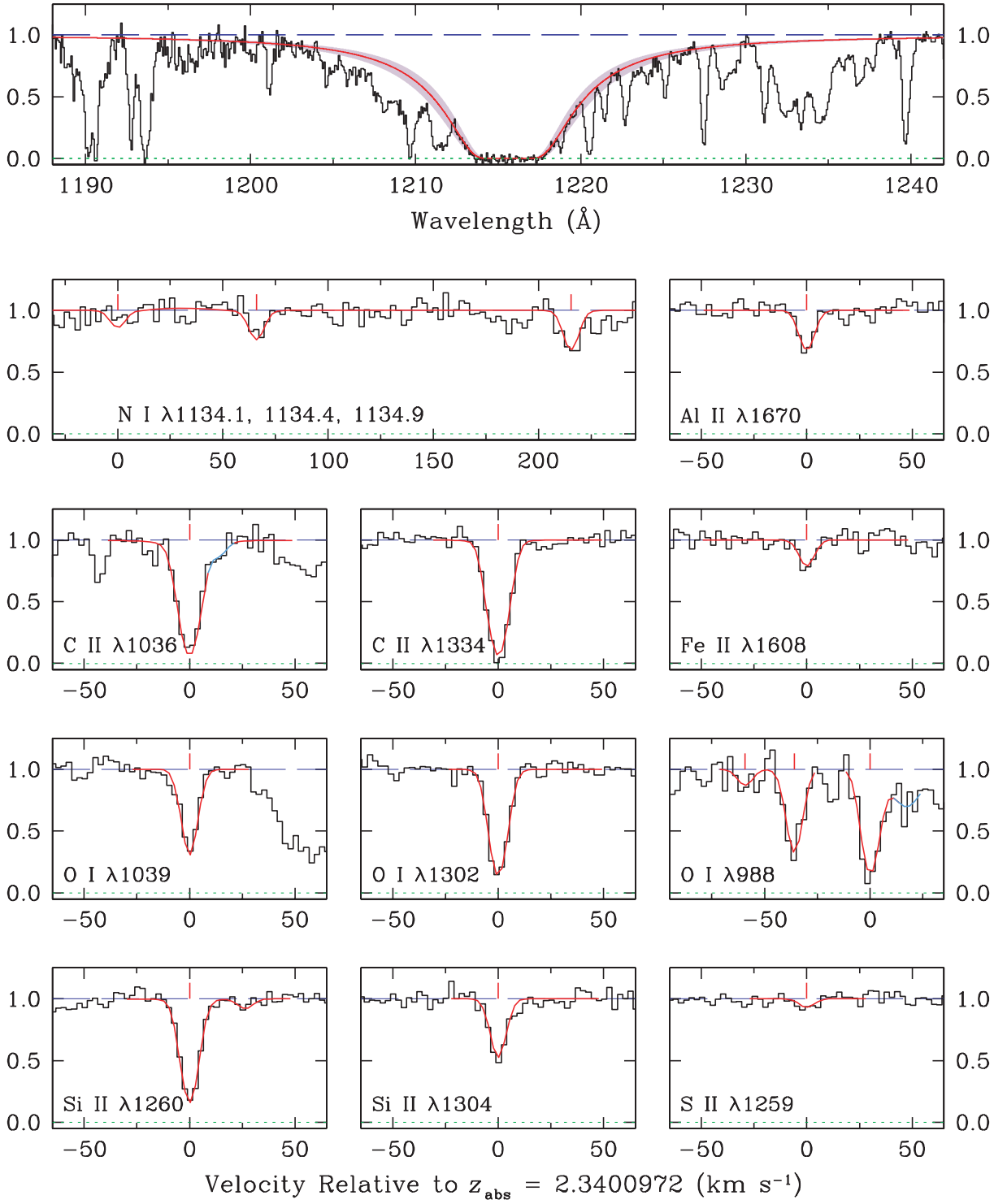

Figure 1. Selected absorption lines in the $z_{abs} = 2.340\,0972$ DLA towards J0035−0918. The data are shown with black histograms, while the red continuous lines are model fits to the line profiles. Top panel: portion of the MagE spectrum of J0035−0918 encompassing the damped Lyα line, together with the theoretical Voigt profile (red line) for a neutral hydrogen column density $\log[N(\mathrm{H\,I})/\mathrm{cm}^{-2}] = 20.55 \pm 0.1$. The remaining panels display portions of the HIRES spectrum near metal lines of interest, together with model profiles generated with VPFIT as described in Section 3.1. This DLA consists of a single absorption component at $z_{abs} = 2.340\,0972$ with a small velocity dispersion, $b = \sqrt{2}\sigma = 2.4\,\mathrm{km\,s^{-1}}$. The weak absorption feature centred at $+26\,\mathrm{km\,s^{-1}}$ in the Si II λ1260.4221 panel is probably Fe II λ1260.533 absorption in the DLA, although its strength is below our 3σ detection limit. The red wings of both C II λ1036 and O I λ988 are blended with a weak Lyα forest line indicated by a continuous blue line. In all plots, the y-axis scale is residual intensity.

Table 1. Metal lines in the $z_{\rm abs} = 2.340\,0972$ DLA towards J0035−0918.

Ion	Wavelength[a] (Å)	f^a	W_0^b (mÅ)	δW_0^c (mÅ)	$\delta W_{0,\rm cont}^d$ (mÅ)
C II	1036.3367	0.118	39	2	1
C II	1334.5323	0.1278	54	2	1
N I	1134.1653	0.0146	<5.3[e]	...	...
N I	1134.4149	0.0278	6.2	1.7	0.5
N I	1134.9803	0.0416	12.5	1.6	0.5
N II	1083.9937	0.111	<4.6[e]	...	...
O I	971.7382	0.0116	24	3	1
O I	988.5778	0.000 553	<6.0[e]	...	...
O I	988.6549	0.0083	23	2	1
O I	988.7734	0.0465	38	3	1
O I	1039.2304	0.009 07	23	2	1
O I	1302.1685	0.048	42	2	1
Al II	1670.7886	1.740	15	2	0.5
Si II	989.8731	0.171	15	2	1
Si II	1193.2897	0.582	28	3	2
Si II	1260.4221	1.18	39	2	0.5
Si II	1304.3702	0.0863	21	2	1
Si II	1526.7070	0.133	34	2	1
S II	1253.805	0.0109	<2.0[e]	...	...
S II	1259.5180	0.0166	3.7	0.8	0.3
Fe II	1260.533	0.0240	<2.5[e]	...	...
Fe II	1608.4509	0.0577	10	2	0.5

[a]Laboratory wavelengths and f-values from Morton (2003).
[b]Rest-frame equivalent width.
[c]Random error on the equivalent width W_0.
[d]Systematic error on W_0 from 1σ uncertainty in the continuum placement.
[e]3σ upper limit on the rest-frame equivalent width.

Table 2. Ion column densities in the $z = 2.340\,0972$ DLA towards J0035−0918.

Ion	$\log N({\rm X})/{\rm cm}^{-2}$
H I	20.55 ± 0.10
C II	15.47 ± 0.15
N I	13.51 ± 0.06
O I	14.96 ± 0.08
Al II	11.73 ± 0.05
Si II	13.41 ± 0.04
S II	≤ 13.08
Fe II	12.98 ± 0.07

With the usual assumption that the ions observed are the dominant stage of the corresponding elements in H I gas, so that corrections for unseen ion stages and/or the presence of ionized gas are negligible (we review this assumption in Section 3.2 below), it is straightforward to deduce the abundances of the elements concerned by simply dividing the column densities in Table 2 by N(H I). Comparison with the solar abundance scale of Asplund et al. (2009) then leads to the abundance pattern listed in Table 3 and illustrated graphically in Fig. 2.

3.2 Ionization corrections

In DLAs, it is usually assumed that the metals within the absorbing H I gas reside in a single dominant ionization stage, X N, so that the total abundance of an element is given by

$$[{\rm X/H}] = [{\rm X\,N/H\,I}] + {\rm IC(X)}, \quad (1)$$

Table 3. Element abundances in the $z = 2.340\,0972$ DLA towards J0035−0918.

Element	$\log\epsilon({\rm X})^a_{\rm DLA}$	$\log\epsilon({\rm X})^{a,b}_{\odot}$	$[{\rm X/H}]^c_{\rm DLA}$
C	6.92	8.43	−1.51
N	4.96	7.83	−2.87
O	6.41	8.69	−2.28
Al	3.18	6.44	−3.26
Si	4.86	7.51	−2.65
S	≤4.53	7.14	≤−2.61
Fe	4.43	7.47	−3.04

[a]$\log\epsilon({\rm X}) = 12 + \log N({\rm X})/N({\rm H})$.
[b]Asplund et al. (2009).
[c]$[{\rm X/H}]_{\rm DLA} \equiv \log\epsilon({\rm X})_{\rm DLA} - \log\epsilon({\rm X})_{\odot}$, with errors as listed in Table 2.

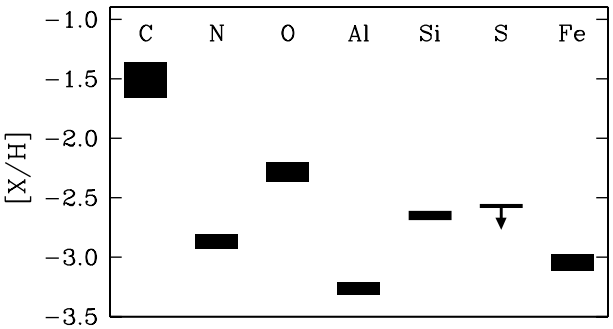

Figure 2. Element abundances in the $z_{\rm abs} = 2.340\,0972$ DLA towards J0035−0918 compared to the solar values as compiled by Asplund et al. (2009). The height of each box represents the uncertainty in each element abundance; the 3σ upper limit for S is indicated by the bar and arrow.

where the ionization correction, IC(X), is typically negligible. In general, it is safe to assume ${\rm IC(X)} \simeq 0.0$ for gas with high N(H I), since the gas is self-shielded from ionizing radiation (e.g. Vladilo et al. 2001). Of course, if the gas does not reside in a single dominant ionization stage, or some amount of X N is associated with H II gas, we may respectively underestimate or overestimate the abundance of a given element [positive or negative IC(X)].

To gauge the extent of such corrections, we used the CLOUDY photoionization software (Ferland et al. 1998) to model the DLA as a slab of gas with uniform density in the range $-3 < \log[n({\rm H})/{\rm cm}^{-3}] < 3$, exposed to the Haardt & Madau (2001) metagalactic ionizing background and the cosmic microwave background, both at the redshift of the DLA. Adopting the solar abundance scale of Asplund et al. (2009), we globally scaled the metals to $\log {\rm Z_{DLA}/Z_{\odot}} = -2.75$ (an approximate average metallicity – see Fig. 2). Once the column density of the DLA was reached, we stopped the simulations and output the resulting ion column densities. Using these computed column densities, we are then able to derive the ionization corrections from equation (1).

The results of our CLOUDY simulations are shown in Fig. 3. The ionization corrections appropriate to the DLA under investigation depend on the volume density of the gas, which can be inferred from the ratio of successive ion stages (see right-hand panel of Fig. 3). The only element for which we have this information is nitrogen and, even then, we can only derive a 3σ upper limit to the N II column density from the 3σ upper limit on the rest-frame equivalent width of the undetected N II λ1084 line (see Table 1), leading to the upper limit $\log N({\rm N\,II})/N({\rm N\,I}) \leq -0.91$. This affords a lower limit on the volume density of $\log[n({\rm H})/{\rm cm}^{-3}] \geq -1.0$ (see right-hand panel

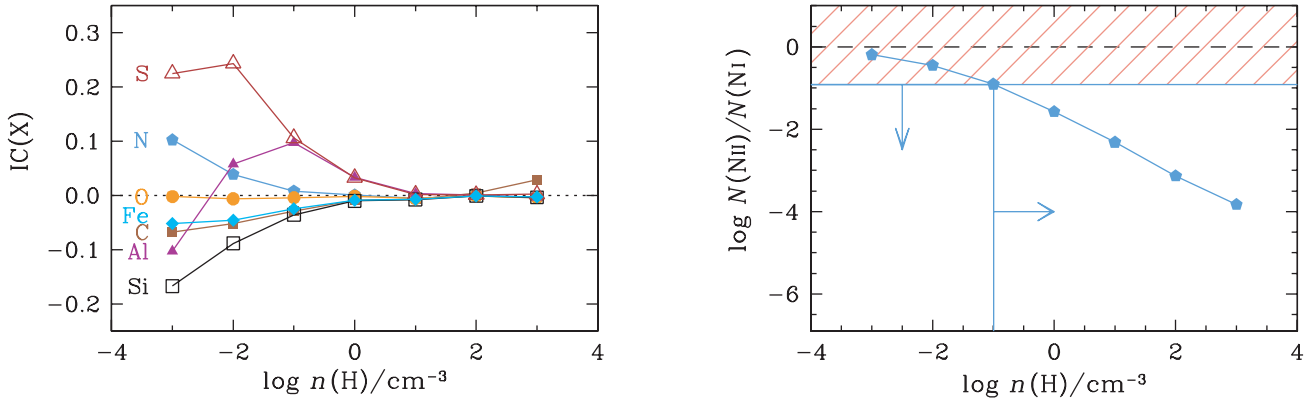

Figure 3. Left-hand panel: ionization corrections, as defined by equation (1), for elements of interest (symbols connected by a solid line), as a function of the volume density of the gas in the $z_{\rm abs} = 2.340\,0972$ DLA. Right-hand panel: ratio of the computed column densities for the successive ion stages of nitrogen (symbols connected by a solid line), plotted as a function of the volume density. The solid horizontal line indicates the upper limit we measure for $\log N({\rm N\,II})/N({\rm N\,I})$, whilst the vertical line with an arrow indicates the corresponding lower limit on the volume density of the gas, $\log [n({\rm H})/{\rm cm}^{-3}] \geq -1.0$. Both plots were produced with CLOUDY photoionization calculations; see the text for further details.

of Fig. 3). Referring now to the left-hand panel of Fig. 3, it can then be seen that, when the gas density is greater than 0.1 cm^{-3}, the ionization corrections for the ions of interest here are indeed small, IC $\lesssim 0.1$ dex. These values are comparable to the uncertainties in the ion column densities (see Table 2) which justifies our assumption that [X/H] $\sim$ [X N/H I], and that ionization corrections are not a serious concern.

It is worth noting, in passing, that even in the absence of several density-sensitive ion ratios, low values of n(H) are in general unlikely in these metal-poor DLAs with such simple velocity structure. The column density $\log[N({\rm H\,I})/{\rm cm}^{-2}] = 20.55$ implies a linear size $l > 1$ kpc along the line of sight if $\log [n({\rm H})/{\rm cm}^{-3}] < -1$. It seems unlikely that the structures giving rise to DLAs with properties similar to that considered here could have such large physical extent while maintaining very quiescent kinematics, with internal velocity dispersions of only a few km s^{-1}.

4 A MASQUERADING CARBON ENHANCEMENT?

Returning to Fig. 2, we note that with [O/H] $= -2.28$ and [Fe/H] $= -3.04$ the $z = 2.340\,0972$ DLA in line to J0035−0918 is among the most metal-poor known (Pettini et al. 2008; Penprase et al. 2010). However, the most striking feature of the abundance pattern in Fig. 2 is the overabundance of carbon relative to all other elements. Thus, for example, [C/O] $=+0.77$, which implies an overabundance of carbon relative to oxygen by a factor of $\sim$6; similarly, [C/Fe] $= +1.53$, or $\sim$35 times solar! Given such extreme values, it is important to consider what factors, if any, may have led us to spuriously overestimate the abundance of carbon. To this end, we performed several tests, which we now discuss. The upshot of these tests is that we could not find any plausible reason why the abundance of carbon would have been significantly overestimated. Thus, readers who are less interested in the details of these checks may skip the rest of this section and move straight to the discussion in Section 5.

4.1 Incorrect background subtraction?

First we considered the possibility that the background may have been oversubtracted in the proximity of the C II absorption lines; if the zero level had been incorrectly determined, this may lead us to overestimate the apparent optical depth of the absorption. While we cannot categorically rule out this possibility, as we do not have any independent measures of the zero level (such as saturated absorption lines with flat cores) in the immediate vicinity of the C II lines, we note the following: (i) there are a number of strongly saturated Lyα absorption lines in the Lyα forest (shortwards of $\lambda_{\rm obs} = 4158$ Å) and none of them shows a systematic offset of their cores from zero residual intensity; (ii) the apparent optical depths of the *two* C II transitions covered by our HIRES spectrum, $\lambda\lambda$1334 and 1036, are mutually consistent (see Fig. 1); thus, if the background level were incorrect, it would have to have been oversubtracted by the same fractional amount of the QSO continuum at these two wavelengths, separated by 995 Å in the observed spectrum (at $z_{\rm abs} = 2.340\,0972$). We also inspected the raw 2D HIRES frames in the region of the two best observed C II and O I lines, $\lambda\lambda$1334 and 1302, and found that they both fall close to the peak of the echelle blaze function, near the centre of the HIRES detector, where the data are of the highest S/N. We conclude that the recorded excess of C is unlikely to be an artefact of the data reduction process.

4.2 Profile fitting 1: gas kinematics

Next we looked critically at the profile fitting procedure. Our VPFIT modelling described in Section 3.1 assumed that the neutrals and singly ionized species arise from gas with the same Doppler parameter. We relaxed this constraint by fitting separately the absorption lines of the first ions (two C II, five Si II lines and one line each of Al II and Fe II) and the neutrals (five O I and two N I lines). In this case, VPFIT converged to best-fitting Doppler parameters of $b = 2.30 \pm 0.09$ for the first ions and $b = 2.6 \pm 0.2$ for the neutrals. With these parameters the C II column density is *higher* by 0.1 dex than the value listed in Table 2 (that is, the value obtained by tying b to be the same for all species), while N(O I) is *lower* by 0.1 dex. The column densities of other elements remain essentially unchanged. In other words, kinematically decoupling neutrals and first ions has the net effect of further *increasing* the [C/O] overabundance relative to the values in Table 3 and Fig. 2. Note also that the above values of b are still consistent within the errors with the best-fitting $b = 2.36 \pm 0.08$ deduced in Section 3.1 by tying all the absorption lines together. Finally, fitting *only* the C II lines, without reference to any other transition, yielded $\log[N({\rm C\,II})/{\rm cm}^{-2}] = 15.42 \pm 0.59$,

which is only 0.05 dex lower than the value listed in Table 2, albeit with a larger error (but with much the same redshift and Doppler parameter: $z_{\rm abs} = 2.340\,096 \pm 0.000\,002$ and $b = 2.4 \pm 0.3$ km s^{-1}).

4.3 Profile fitting 2: instrumental resolution

In order to compare theoretical and observed absorption line profiles, VPFIT requires knowledge of the instrumental broadening function, normally assumed to be a Gaussian with FWHM corresponding to the spectral resolution. The nominal resolution of spectra recorded through the 1.148-arcsec wide entrance slit of HIRES employed in our observations is FWHM =8.1 km s^{-1} (see http://www2.keck.hawaii.edu/inst/hires/), but this applies to a uniformly illuminated slit. Since the seeing was consistently better than 1.148 arcsec during our observations of J0035−0918, it is likely that the actual resolution of our data is somewhat better than the nominal value. The narrowest features in the spectrum of J0035−0918 are the metal absorption lines of the $z_{\rm abs} = 2.340\,0972$ DLA themselves. We therefore estimated the true spectral resolution – measured by the Doppler parameter $b_{\rm instr} \equiv 0.6006$ FWHM – by varying $b_{\rm instr}$ in small steps from 5.0 to 3.7 km s^{-1} (i.e. between FWHM =8.3 and 6.2 km s^{-1}), fitting all of the absorption lines as described in Section 3.1, and minimizing the χ^2 between the model and observed profiles as a function of $b_{\rm instr}$. This procedure gave a well-defined $b_{\rm instr,min} = 4.4$ km s^{-1}, corresponding to FWHM = 7.3 km s^{-1}, or $R = 41\,000$, which is the value used in all the profile fitting described in Sections 3.1 and 4.2.

It is obviously important to test the sensitivity of our results to the value of $b_{\rm instr}$ adopted. Within the range of values tested, $b_{\rm instr} = 5.0$–3.7 km s^{-1}, the column density of C II and the corresponding element ratios changed by no more than ±0.1 dex compared to the values in Table 2 which refer to the case $b_{\rm instr,min} = 4.4$ km s^{-1}. On the basis of the tests carried out in this and the preceding subsection, we conclude that the overabundance of carbon is not an artefact of the profile fitting analysis of the absorption lines.

4.4 Monte Carlo simulations

The $z = 2.340\,0972$ DLA in J0035−0918 is unique so far in showing such a marked overabundance of carbon. More typically, DLAs with [O/H] < -2 have [C/O] $\simeq -0.2$ and at most [C/O] $\simeq 0.0$ [i.e. (C/O) = (C/O)$_\odot$; Pettini et al. 2008; Cooke R. et al. (in preparation)]. It is therefore worthwhile considering to what extent a solar C/O ratio is excluded by our data. We illustrate this test in Fig. 4,

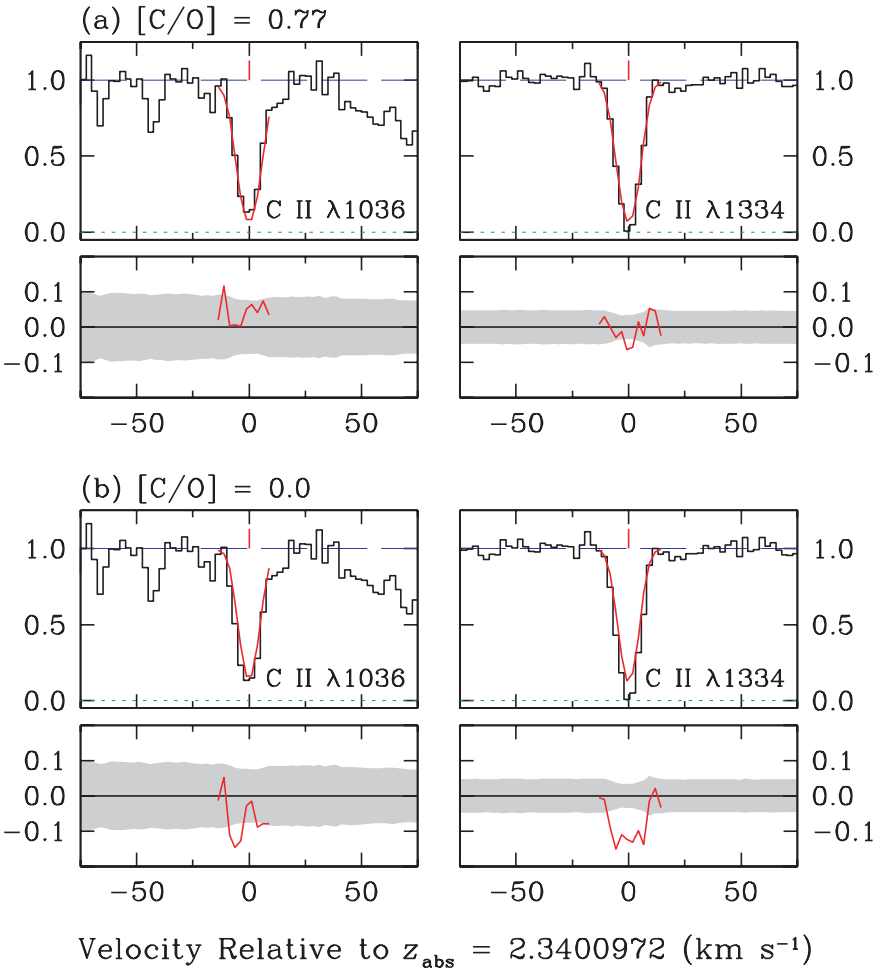

Figure 4. Comparison between observed C II line profiles (black histograms) and theoretical profiles computed with VPFIT (red continuous lines). Below each plot we also show the difference between computed and observed residual intensities (red lines) compared with the 1σ error spectrum of the data (grey area). (a) Best-fitting model as described in Section 3.1 with $\log[N({\rm C\,II})/{\rm cm}^{-2}] = 15.47$ as in Table 2. (b) Best-fitting model obtained by forcing $\log[N({\rm C\,II})/{\rm cm}^{-2}] = 14.70$ so that [C/O] = 0.0 (see text for further details). This model provides a poorer fit to both C II absorption lines, as demonstrated by the mismatch between the model subtracted from the data and the 1σ error spectrum (bottom panels).

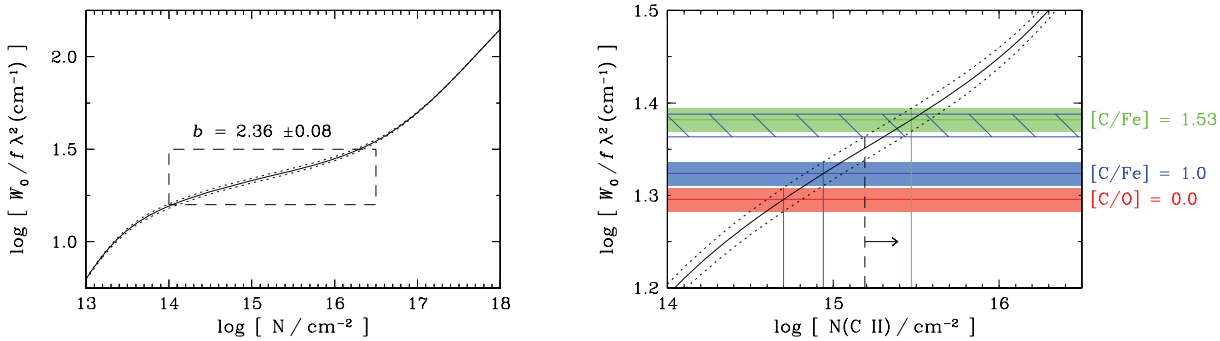

Figure 5. Left-hand panel: curve of growth for the $z_{\rm abs} = 2.340\,0972$ DLA in line to J0035−0918, with Doppler parameter $b = 2.36 \pm 0.08$ km s^{-1}. The dashed box shows the region reproduced on an expanded scale in the right-hand panel. Right-hand panel: equivalent width comparison. The continuous black line is a portion of the curve of growth for Doppler parameter $b = 2.36$ km s^{-1}, with the short-dash lines indicating the uncertainty $\delta b = \pm 0.08$ km s^{-1}. The red, blue and green horizontal bands show the corresponding ranges in equivalent width W_0(C II λ1334) appropriate to element ratios [C/O] = 0.0, [C/Fe] = +1.0 and [C/Fe] = +1.53, respectively. Only the last of these (green band) matches the measured equivalent width of C II λ1334, indicated by the blue hatched horizontal band. A strict lower limit [C/Fe] ≥ +1.25 (vertical long-dash line with right-pointing arrow) is obtained by considering the lower bound on W_0(C II λ1334) and upper bound on b.

where we compare the line profiles for the two C II absorption lines generated with (upper panels) the best-fitting model returned by VPFIT, and (lower panels) a model in which N(C II) has artificially been fixed at the column density corresponding to [C/O] = 0.0 (that is $\log[N({\rm C\,II})/{\rm cm}^{-2}] = 14.70$ as opposed to 15.47 as in Table 2). While the former results in a χ^2/d.o.f. = 13.9/22, the latter fits are worse, with χ^2/d.o.f. = 86.6/22. The higher value of χ^2 is reflected by the higher residuals, both in the core and the wings of the C II λ1334 line in particular, as can be appreciated from close examination of Fig. 4. The noisier C II λ1036 line is less instructive in this context, partly because of blending with Lyα forest lines.

It may be surprising to some to see what subtle changes in the line profiles result from changing N(C II) by a factor of ∼6. The reason is that the two C II absorption lines are close to saturation and, as they approach the flat part of the curve of growth, their equivalent widths only increase slowly with rising column density. In the present case, the curve of growth for the metal lines in the $z_{\rm abs} = 2.340\,0972$ DLA towards J0035−0918 (reproduced in Fig. 5) is well constrained by the relative strengths of six O I and five Si II transitions of widely differing f-values (see Table 1). Since the column densities of both O I and Fe II are fixed by optically thin transitions (i.e. independent of the Doppler parameter), the ratios [C/O] and [C/Fe] depend only on the C II column density. In the right-hand panel of Fig. 5, we compare the measured equivalent width of C II λ1334 (indicated by the blue hatched region) with the values expected if [C/O] = 0.0 (red), [C/Fe] = +1.0 (blue) and [C/Fe] = +1.53 (green). Only in this last case ([C/Fe] = +1.53) do we recover the measured W_0(C II λ1334), whereas the strength of the line is underpredicted in the other two cases illustrated. The partially blended C II λ1036 line is not instructive in this equivalent width test which, by its nature, is less sensitive than the pixel-by-pixel line profile analysis illustrated in Fig. 4.

Figs 4 and 5 offer a clearer view of the carbon-enhanced nature of this DLA, while at the same time highlighting the subtle differences in the absorption line profiles when lines are on the flat part of the curve of growth. Thus, it is reasonable to question whether the differences between the line profiles computed with [C/O] = 0.0 and the observed profiles, most evident for C II λ1334 in the bottom right-hand set of panels in Fig. 4, may be simply due to statistical fluctuations. We tested this possibility with a Monte Carlo-type approach. We synthesized 100 pairs of C II λλ1036, 1334 line profiles, all corresponding to [C/O] = 0.0 and with the best-fitting Doppler parameter ($b = 2.36 \pm 0.08$). We perturbed these line profiles with Gaussian distributed errors from the observed 1σ error spectrum, and then used VPFIT to fit each of these 100 pairs of C II lines (together with the observed line profiles of the other ions) and deduce 100 new values of N(C II). Using the simultaneously derived O I column density (which is essentially unchanged since it is constrained by weaker transitions), we calculated the [C/O] ratio for all of our realizations to determine how often one would expect to observe [C/O] ≥ 0.77 if the true [C/O] ratio were solar. The results of this Monte Carlo approach are shown in Fig. 6. In none of the simulations was a value of [C/O] as high as +0.77 recovered. The distribution of recovered values is symmetric about the input value [C/O] = 0.0 with a dispersion $\sigma = 0.087$. Thus, if the [C/O] ratio in the $z_{\rm abs} = 2.340\,0972$ DLA were indeed solar (which in itself is higher or as high as observed in any other DLA up to now), our data would constitute a ∼9σ deviation, which is very unlikely indeed.

In conclusion, none of the tests we have performed can explain away the C overabundance we have uncovered. The most straightforward interpretation of the data is that we have identified a DLA

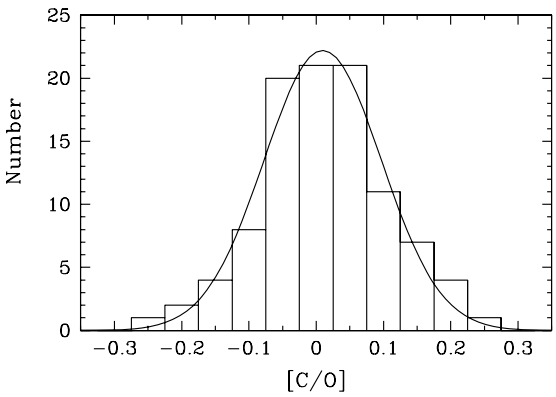

Figure 6. Histogram of the values of [C/O] recovered from 100 Monte Carlo realizations with input [C/O] = 0.0 in which the synthetic C II λλ1334, 1036 line profiles were perturbed with a random realization of the error spectrum. The overlaid Gaussian fit to the results has a dispersion $\sigma = 0.087$, which implies that our measured value [C/O] = +0.77 would be a ∼9σ random fluctuation if the [C/O] ratio were solar in the $z_{\rm abs} = 2.340\,0972$ DLA.

with a marked overabundance of C, comparable to that so far found only in carbon-enhanced metal-poor stars of the Milky Way.

5 A CARBON-ENHANCED METAL-POOR DLA

As already mentioned, this is the first example of a DLA meeting the conventional definition of CEMP stars, [C/Fe] $> +1.0$. While it is the only such case in the survey by Cooke R. et al. (in preparation), which includes a dozen DLAs with [Fe/H] < -2, it is nevertheless very hard to draw conclusions regarding the frequency of CEMP DLAs. The reason stems from the difficulties associated with measuring the C II column density; the C II $\lambda\lambda$1036 and 1334 absorption lines are almost always saturated in damped Lyα absorption systems, even at low metallicities. CEMP DLAs may thus be easily overlooked.

The discovery of a gaseous, high redshift, counterpart to CEMP stars of the Galactic halo is a breakthrough with potentially very important consequences. As mentioned in the Introduction, interpretations still differ as to the origin of the carbon enhancement in VMP stars, but the favoured explanation involves mass transfer from an AGB companion, at least for the members of the CEMP class which also exhibit enhancements in *s*-process elements. The situation is less clear-cut for the CEMP stars with no such enhancement, the CEMP-no stars. On the one hand, there may be a continuous link between this class and the CEMP-s class (Masseron et al. 2010), so that in some CEMP-no stars the carbon enhancement may also be due to mass transfer from an unseen companion. On the other hand, the binary transfer scenario cannot readily explain why the fraction of all metal-poor stars that exhibit a carbon-enhancement increases with decreasing metallicity (Beers & Christlieb 2005). In fact, the only physical model so far put forward that can explain this increased fraction *requires* a high carbon yield from metal-free stars to efficiently cool low metallicity gas and drive the transition from Population III to Population II star formation (Frebel, Johnson & Bromm 2007).

While CEMP-no stars in the Galactic halo may have more than one origin, the same ambiguities do not apply to the carbon enhancement in the DLA presented here, where we have an entire cloud overabundant in carbon (below we place limits to the total mass of carbon involved). Rather, what we presumably see in the DLA is the initial chemical composition of the gas from which CEMP stars would subsequently form. In this case, the pattern of element abundances revealed gives strong clues to the nature of the earlier generation of stars (and supernovae) which seeded the DLA cloud with its metals.

We explore these ideas further by comparing the abundance pattern of the DLA with those of halo stars of similar metallicity and with calculations of element yields from metal-free and metal-poor stars. In this endeavour, we are limited by the small number of elements whose abundances we have been able to measure, but this is an inevitable consequence of the low metallicity of this DLA. While it would be instructive to know the abundances of other Fe-peak elements, such as Cr and Zn for example, the absorption lines of these species would require S/N $\gtrsim 500$ for 5σ detections![5] Realistically, only Mg and S are within reach of dedicated future observations, and there is certainly no hope of measuring directly the abundances of neutron capture elements in the DLA.

5.1 Comparison with stellar abundances

In order to compare the relative abundances of the elements measured in the DLA with the corresponding values in Galactic halo stars, we median-combined the abundances of all CEMP stars with Fe/H within a factor of 2 of the DLA ($-3.34 \leq$ [Fe/H] ≤ -2.74) from the recent compilation of Frebel (2010). We then calculated the dispersion in each abundance using the IDL routine ROBUST_SIGMA[6] which determines the median absolute deviation (unaffected by outliers) of a set of measurements, and then appropriately weights the data to provide a robust estimate of the sample dispersion (Hoaglin, Mosteller & Tukey 1983, cf. Cooke et al. 2010).

Fig. 7 illustrates three comparisons. In the top panel, the DLA abundance pattern (solid black boxes) is shown together with that of the 'average' population of all CEMP stars (open magenta boxes), while in the middle panel the comparison is restricted to CEMP-no stars. Clearly CEMP stars, of both flavours, are a heterogeneous population, exhibiting wide ranges in the ratios of the elements considered here. On the basis of the limited evidence available, it appears that the C/Fe ratio in our DLA is a better match to the values seen in the subset of CEMP-no stars than to the more extreme values encountered in some CEMP stars. Other elements ratios are less straightforward to interpret.

Nitrogen, for example, is evidently less abundant in the DLA compared to CEMP stars by $\sim$2 orders of magnitude! However, it is difficult to draw firm conclusions from this discrepancy, because the abundance of N is notoriously difficult to measure in metal-poor stars where it relies on the analysis of molecular bands of NH or CN, each with its own disadvantages (see e.g. Asplund 2005). The largest uncertainty arises from the assumed 1D (rather than 3D) model atmospheres; correcting for 3D effects can change the deduced values of N/H by ~ -0.5 dex. (Note that similar corrections also apply to C/H when derived from molecular bands of CH or C_2; Collet, Asplund & Trampedach 2007). Furthermore, the photospheric N/H we measure today is unlikely to reflect the N abundance of the gas cloud that gave birth to the star; during the star's evolution it will become self-polluted by its own nucleosynthesis (e.g. through CN cycling or rotational mixing), which is likely emphasized by the high seed C abundance. Thus, a comparison between stellar and DLA nitrogen abundances is not very instructive.

Comparing the oxygen abundances in CEMP stars and the DLA is similarly problematic. The statistics are very poor (see Fig. 7) and it is well known that different spectral features used to deduce O/H in the metal-poor regime give discordant answers (García Pérez et al. 2006). Significant departures from local thermodynamic equilibrium (LTE) become important when measuring the O abundance from the infrared triplet at 777 nm in the metal-poor regime ([Fe/H] < -2.5), leading to non-LTE corrections of the order of -0.5 to -1.0 dex (Fabbian et al. 2009b). Similarly, the oxygen abundance determined from the UV OH lines is subject to large 3D corrections of up to -0.9 dex when [Fe/H] ≤ -3.0 (Asplund 2005). Clearly, it will be important to re-examine this issue once samples of CEMP stars have grown to include more cases where [O/Fe] has been measured with confidence.

Finally, Fig. 7 demonstrates that there is a reasonably good match between CEMP stars and the DLA in the elements Al and Si, particularly for the CEMP-no stars. In this context, we point out that significant (positive) non-LTE corrections to Al/H may apply for stars in this metallicity regime (see e.g. Asplund 2005). To address

[5] Assuming [Cr/Fe] = [Zn/Fe] = 0.0 .

[6] Available from http://idlastro.gsfc.nasa.gov/homepage.html.

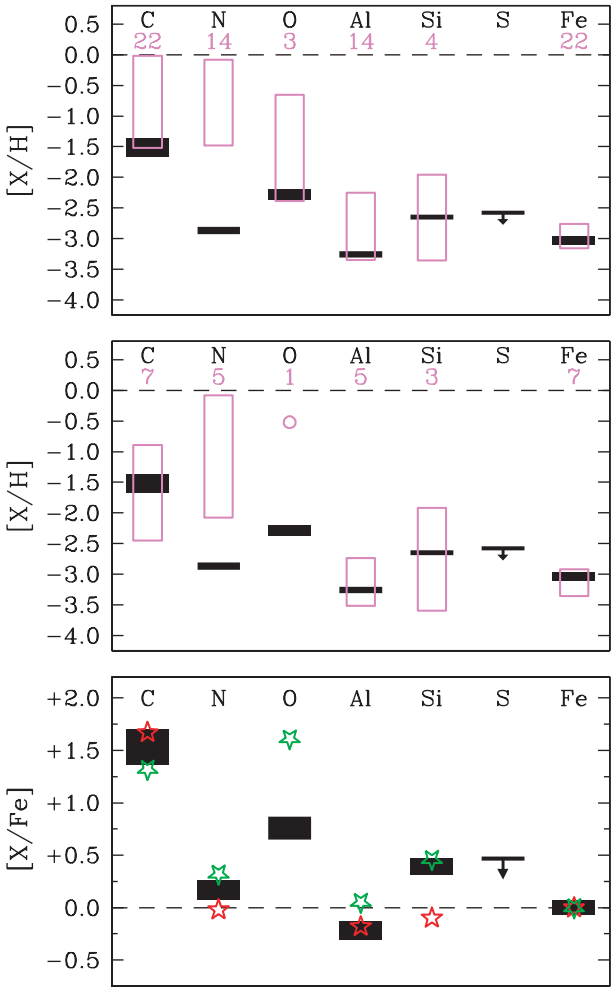

Figure 7. Comparison of element abundances in the $z_{abs} = 2.340\,0972$ DLA (filled black boxes) and in Galactic halo stars with an Fe abundance within a factor of 2 of the DLA (open magenta boxes). The numbers below the element labels indicate the number of stars that contributed to the determination of the 'typical' stellar abundances, and the heights of the magenta boxes reflect the dispersion of each set of measurements. Top panel: comparison with all CEMP stars that have $-3.34 \leq$ [Fe/H] ≤ -2.74. Middle panel: comparison with CEMP-no stars that have $-3.34 \leq$ [Fe/H] ≤ -2.74. For this case, the oxygen abundance of a single CEMP-no star is shown by the open circle. Lower panel: comparing the DLA abundance pattern with the stellar abundance patterns of HE 0143−0441 (red symbols; a CEMP-s star with [Fe/H] $= -2.21$, [Ba/Fe] $= +0.62$ from Cohen et al. 2004) and BD+44°493 (green symbols; a CEMP-no star with [Fe/H] $= -3.73$, [Ba/Fe] $= -0.55$ from Ito et al. 2009). Note that in this last panel, we have plotted [X/Fe] as opposed to [X/H]. In all panels the dashed line represents the solar abundance.

this issue, we first identified those CEMP stars in the Frebel (2010) compilation whose Al abundances were derived assuming LTE. We then applied non-LTE corrections to Al based on the Andrievsky et al. (2008) estimates, which amounted to a typical correction of the order of +0.6. The Al abundances for the 'typical' CEMP and CEMP-no star presented in Fig. 7 should thus correspond to the (approximate) non-LTE values.

Finally, in the lower panel of Fig. 7 we compare the element ratios (relative to Fe) in the DLA with the values measured for two CEMP stars selected from the compilation by Frebel (2010) because they most closely match the relative abundances in the DLA. It is certainly plausible that stars forming out of this DLA gas would share many chemical similarities – at least for the elements considered here – with these two stars of the Milky Way Galactic halo.

5.2 Comparison with model yields for metal-free stars

With a metallicity [Fe/H] of only 1/1000 solar, it is conceivable that the chemical composition of the DLA gas reflects the element yields of only a few prior generations of stars. It is thus of interest to compare the abundance pattern in Fig. 2 with calculations of nucleosynthesis by metal-free, or low-metallicity, stars. Calculations of yields from metal-free stars (commonly referred to as Population III stars), aimed in particular at interpreting the element ratios seen in VMP stars, have focused on models which include 'mixing and fallback' (e.g. Umeda & Nomoto 2002, 2003; Heger & Woosley 2010). These scenarios involve core-collapse supernovae where the elements synthesized in the inner regions of the star are mixed by some process (several possibilities have been put forward); a fraction of the mixed material subsequently falls back on to the central remnant while the rest is ejected into interstellar space.

Such models are illustrative, rather than predictive, since the parameters describing the boundaries of the mixing region and the fraction of the mixed material which is ejected cannot be derived from first principles, and are instead parametrized and suitably adjusted to fit the observed stellar abundances (e.g. Tominaga, Umeda & Nomoto 2007). A string of recent models that employ a more physically motivated prescription of fallback (Heger & Woosley 2010) have also investigated the effects of mixing due to the Rayleigh–Taylor instability (Joggerst et al. 2009) together with rotationally induced mixing in 2D (Joggerst et al. 2010a) and 3D (Joggerst et al. 2010b). By and large, a general feature of these models is that an abundance pattern similar to that found here in the DLA, including the carbon enhancement and the marked odd–even effect (see Fig. 2), can be reproduced with low-energy explosions, such as those giving rise to the faint supernova branch (see fig. 1 of Tominaga et al. 2007, and fig. 11 of Heger & Woosley 2010), and a moderate degree of mixing and fallback. For example, in the mixing-fallback model considered by Tominaga (2010), enrichment with the elements ejected by a single 25 $M_\odot$ star of zero metallicity, exploding as a core-collapse supernova with an energy $E_{SN} \sim 10^{51}$ erg, provides a remarkably good fit to the relative element abundances measured in the DLA (Kobayashi et al., in preparation).

It remains to be established whether a zero initial metallicity (i.e. Population III) is actually required to match the observations, or whether a similar abundance pattern could also be reproduced by models with low, but non-zero, initial metallicity. An alternative to the mixing and fallback model has been proposed by the Geneva group whose work places more emphasis on the effects of rotation to provide the mixing and the trigger for mass loss in VMP stars (e.g. Meynet et al. 2006; Hirschi 2007; Meynet et al. 2010). Whilst these models are physically well-motivated, the rather high nitrogen yield predicted by some models contrasts with the relatively low [N/C] and [N/O] observed in this DLA. This may in turn place interesting constraints on the rotation velocities of the metal-free stars that may have seeded the DLA with its metals. Only recently has rotation been included in zero-metallicity progenitors under the mixing-fallback scenario (Joggerst et al. 2010a). It should be possible to assess better the effects of rotation on the yield from zero-metallicity progenitors

as these stellar models improve and as the samples of CEMP DLAs grow.

5.3 How many supernovae?

It is truly intriguing that an *entire* cloud of neutral gas is so highly enhanced in carbon and shows such a clear-cut odd–even effect, if both are indeed characteristic of Population III supernova yields. In this context, it is of interest to estimate the mass of carbon involved. With the assumption of spherical symmetry, the mass of singly ionized carbon in the DLA is given by

$$M(\mathrm{C\,II}) = 12\,M(\mathrm{H\,I})\,\frac{N(\mathrm{C\,II})}{N(\mathrm{H\,I})} \tag{2}$$

$$M(\mathrm{C\,II}) = 2\,\pi\,m_{\mathrm{H}}\frac{N(\mathrm{H\,I})^2 N(\mathrm{C\,II})}{n(\mathrm{H})^2} \tag{3}$$

$$M(\mathrm{C\,II}) \leq 200\left(\frac{n(\mathrm{H})}{0.1\,\mathrm{cm}^{-3}}\right)^{-2} M_{\odot}, \tag{4}$$

where m_{H} is the mass of a hydrogen atom and n(H) is the volume density (cm^{-3}). The corresponding mass of neutral gas in the DLA is

$$M_{\mathrm{DLA}} = 1.3\,m_{\mathrm{H}}\,\frac{4\pi}{3}\,\frac{N(\mathrm{H\,I})^3}{8\,n(\mathrm{H})^2} \tag{5}$$

$$M_{\mathrm{DLA}} \leq 2.5\times10^{6}\left[\frac{n(\mathrm{H})}{0.1\,\mathrm{cm}^{-3}}\right]^{-2} \mathrm{M}_{\odot}. \tag{6}$$

Since C is mostly singly ionized in DLAs, equation (4) implies an upper limit of 200 $\mathrm{M}_{\odot}$ to the total mass of ^{12}C in the DLA. However, the inverse square dependence of M(C II) on the gas density allows substantially lower values of M(C II). In Section 3.2, it was shown that our lower limit $n(\mathrm{H}) \geq 0.1$ cm^{-3} was based on the non-detection of N II absorption, and that higher densities are likely given the very low velocity dispersion of the gas. If, for example, $n(\mathrm{H}) \simeq 1$ cm^{-3}, which would imply a linear extent of the DLA of 100 pc along the line of sight, then the implied mass of ^{12}C would be reduced to only 2 $\mathrm{M}_{\odot}$. For comparison, the total mass of ^{12}C ejected by the single 25 $\mathrm{M}_{\odot}$ Population III star in the model by Tominaga (2010) is $\sim$0.2 $\mathrm{M}_{\odot}$. The models by Heger & Woosley (2010) anticipate a similar ejected mass of ^{12}C ($\sim$0.3 $\mathrm{M}_{\odot}$) for a comparable explosion energy and progenitor mass. Thus, we may indeed be seeing the elements synthesized by only a few supernovae in the chemical enrichment of the DLA considered here.

In conclusion, we speculate that the $z_{\mathrm{abs}} = 2.340\,0972$ DLA in front of the QSO J0035−0918 may well be the much sought after 'missing link' between the first, zero-metallicity, stars and the most metal-poor stars in the halo of our Galaxy. Its low metallicity of 1/1000 solar in Fe, coupled with an overabundance of C and a marked odd–even effect in the relative abundances of the few elements that could be measured, are all consistent with the yields produced by models of Population III stars which explode as core-collapse supernovae of relatively low energy. The mass of newly synthesized elements may be that produced by only a few such supernovae, depending on the unknown volume density of the gas in the DLA. In this scenario, the gas we see as a DLA at high redshift may be the material from which a subsequent generation of stars formed, with a chemical composition similar to that seen in CEMP-no stars of the Galactic halo.

6 SUMMARY AND CONCLUSIONS

In the course of our programme to study the most metal-poor DLAs and, in particular, to measure the abundances of the CNO group of elements, we have uncovered a DLA, at $z_{\mathrm{abs}} = 2.340\,0972$ towards the $z_{\mathrm{em}} = 2.42$ SDSS QSO J0035−0918, whose chemical composition is consistent with that produced from exploding Population III stars. From the analysis of medium- and high-resolution spectra of this DLA, we draw the following conclusions.

(i) The metal absorption lines associated with the DLA are formed in quiescent gas, consisting of a single absorption component with a small Doppler parameter $b = 2.4\,\mathrm{km\,s^{-1}}$.

(ii) The metallicity of the DLA, as measured from Fe, is very low: [Fe/H] $= -3.04 \pm 0.17$, or $\sim$1/1000 solar.

(iii) The DLA exhibits a strong enhancement of the abundance of carbon relative to all other metals covered by our data: N, O, Al, Si, S and Fe. We measure [C/Fe] $= +1.53$, a factor of $\sim$20 greater than observed in any other DLA up to now. Adopting the defining criterion for carbon-enhanced metal-poor stars in the Galactic halo, [C/Fe] $> +1.0$, this is the first example of an analogous carbon-enhanced DLA. We also deduce [C/O] $= +0.77$, whereas in all other DLAs with [Fe/H] < -2 studied up to now [C/O] $\lesssim 0.0$.

(iv) The DLA also exhibits a clear odd–even effect, which implies a low neutron excess, and hence presumably low abundances of neutron-capture elements. When its chemical composition is compared with that of Galactic carbon-enhanced metal-poor stars which do not exhibit an excess of neutron-capture elements, a good match is found for some element ratios (C/Fe, Al/Fe and Si/Fe). N and O are significantly less abundant, compared to Fe, in the DLA than in most CEMP stars, but it is difficult to draw definite conclusions for these two elements which are notoriously difficult to measure in VMP stars.

(v) The abundance pattern we observe for this DLA is consistent with enrichment from a population of $\sim$20–50 $\mathrm{M}_{\odot}$ metal-free, or extremely metal-poor, stars that ended their lives as core-collapse supernovae with modest explosion energies. We estimate the total mass of ^{12}C within the DLA to be $\leq$200 $\mathrm{M}_{\odot}$. This upper limit could be constrained further with higher S/N spectra that would permit a measure of the column density of N II and other successive ion stages whose ratios are density-dependent. The steep dependence of $M(^{12}\mathrm{C})$ on the gas density allows the possibility that we may be seeing the chemical enrichment produced by only a few prior supernovae.

(vi) We speculate that the gas in this DLA may be the 'missing link' between the yields of Population III stars, and their later incorporation in the CEMP-no class of carbon-enhanced metal-poor stars. We note, however, that the carbon enhancement in some CEMP-no stars could also be produced by other means. Long-term radial velocity monitoring of CEMP-no stars will confirm or deny their association with a now extinct companion.

The results presented here emphasize the importance of further observations of DLAs with [Fe/H] ≤ -3 to complement the work being carried out on the most metal-poor stars. Such DLAs may be the most suitable environments for measuring the true yields from zero- or low-metallicity stars, free from the complications of stellar abundance measurements and the possibility that these stars are polluted by an unseen binary companion, or self-polluted by their own nucleosynthesis. The extremely metal-poor regime for DLAs is yet to be thoroughly explored with high-resolution and high S/N spectra – who knows what may lurk there!

ACKNOWLEDGMENTS

We are grateful to the staff at the Keck and Magellan telescopes for their assistance with the observations, and to Tom Barlow, George Becker, Bob Carswell, Gary Ferland and Michael Murphy for providing much of the software used in the reduction and analysis of the data. We wish to thank Poul Nissen and Chris Tout for useful discussions regarding the stellar abundances. Chiaki Kobayashi and Nozomu Tominaga kindly helped with the interpretation of the results. A prompt and comprehensive referee report significantly improved the paper. We thank the Hawaiian people for the opportunity to observe from Mauna Kea; without their hospitality, this work would not have been possible. RC is jointly funded by the Cambridge Overseas Trust and the Cambridge Commonwealth/Australia Trust with an Allen Cambridge Australia Trust Scholarship. CCS's research is partly supported by grants AST-0606912 and AST-0908805 from the US National Science Foundation.

REFERENCES

Akerman C. J., Carigi L., Nissen P. E., Pettini M., Asplund M., 2004, A&A, 414, 931
Akerman C. J., Ellison S. L., Pettini M., Steidel C. C., 2005, A&A, 440, 499
Andrievsky S. M., Spite M., Korotin S. A., Spite F., Bonifacio P., Cayrel R., Hill V., François P., 2008, A&A, 481, 481
Aoki W., Beers T. C., Christlieb N., Norris J. E., Ryan S. G., Tsangarides S., 2007, ApJ, 655, 492
Asplund M., 2005, ARA&A, 43, 481
Asplund M., Grevesse N., Sauval A. J., Scott P., 2009, ARA&A, 47, 481
Becker G. D., Sargent W. L. W., Rauch M., Simcoe R. A., 2006, ApJ, 640, 69
Beers T. C., Christlieb N., 2005, ARA&A, 43, 531
Beers T. C., Preston G. W., Shectman S. A., 1992, AJ, 103, 1987
Cayrel R. et al., 2004, A&A, 416, 1117
Christlieb N., Green P. J., Wisotzki L., Reimers D., 2001, A&A, 375, 366
Christlieb N. et al., 2002, Nat, 419, 904
Cohen J. G. et al., 2004, ApJ, 612, 1107
Collet R., Asplund M., Trampedach R., 2007, A&A, 469, 687
Cooke R., Pettini M., Steidel C. C., King L. J., Rudie G. C., Rakic O., 2010, MNRAS, 409, 679
Erni P., Richter P., Ledoux C., Petitjean P., 2006, A&A, 451, 19
Fabbian D., Nissen P. E., Asplund M., Pettini M., Akerman C., 2009a, A&A, 500, 1143
Fabbian D., Asplund M., Barklem P. S., Carlsson M., Kiselman D., 2009b, A&A, 500, 1221
Ferland G. J., Korista K. T., Verner D. A., Ferguson J. W., Kingdon J. B., Verner E. M., 1998, PASP, 110, 761
Frebel A., 2010, Astron. Nachr., 331, 474
Frebel A. et al., 2005, Nat, 434, 871
Frebel A., Johnson J. L., Bromm V., 2007, MNRAS, 380, L40
Fujimoto M. Y., Ikeda Y., Iben I., Jr, 2000, ApJ, 529, L25
García Pérez A. E., Asplund M., Primas F., Nissen P. E., Gustafsson B., 2006, A&A, 451, 621
Haardt F., Madau P., 2001, in Neumann D. M., Tran J. T. V., eds, XXIst Moriond Astrophys. Meeting, Clusters of Galaxies and the High Redshift Universe Observed in X-ray. Editions Frontiéres, Paris, p. 64
Heger A., Woosley S. E., 2010, ApJ, 724, 341
Hirschi R., 2007, A&A, 461, 571
Hoaglin D. C., Mosteller F., Tukey J. W., 1983, Understanding robust and exploratory data analysis. Wiley, New York
Ito H., Aoki W., Honda S., Beers T. C., 2009, ApJ, 698, L37
Joggerst C. C., Woosley S. E., Heger A., 2009, ApJ, 693, 1780
Joggerst C. C., Almgren A., Bell J., Heger A., Whalen D., Woosley S. E., 2010a, ApJ, 709, 11
Joggerst C. C., Almgren A., Woosley S. E., 2010b, ApJ, 723, 353
Ledoux C., Petitjean P., Fynbo J. P. U., Møller P., Srianand R., 2006, A&A, 457, 71
Lucatello S., Beers T. C., Christlieb N., Barklem P. S., Rossi S., Marsteller B., Sivarani T., Lee Y. S., 2006, ApJ, 652, L37
Marshall J. L. et al., 2008, SPIE, 7014, 701454
Masseron T., Johnson J. A., Plez B., van Eck S., Primas F., Goriely S., Jorissen A., 2010, A&A, 509, A93
Meynet G., Ekström S., Maeder A., 2006, A&A, 447, 623
Meynet G., Hirschi R., Ekstrom S., Maeder A., Georgy C., Eggenberger P., Chiappini C., 2010, A&A, 521, A30
Morton D. C., 2003, ApJS, 149, 205
Murphy M. T., Curran S. J., Webb J. K., Ménager H., Zych B. J., 2007, MNRAS, 376, 673
Norris J. E., Christlieb N., Korn A. J., Eriksson K., Bessell M. S., Beers T. C., Wisotzki L., Reimers D., 2007, ApJ, 670, 774
Penprase B. E., Prochaska J. X., Sargent W. L. W., Toro-Martinez I., Beeler D. J., 2010, ApJ, 721, 1
Pettini M., King D. L., Smith L. J., Hunstead R. W., 1997, ApJ, 478, 536
Pettini M., Zych B. J., Steidel C. C., Chaffee F. H., 2008, MNRAS, 385, 2011
Pontzen A. et al., 2008, MNRAS, 390, 1349
Prochaska J. X., Wolfe A. M., 2002, ApJ, 566, 68
Prochaska J. X., Chen H.-W., Wolfe A. M., Dessauges-Zavadsky M., Bloom J. S., 2008, ApJ, 672, 59
Siess L., Goriely S., Langer N., 2004, A&A, 415, 1089
Tominaga N., 2010, in Whalen D., ed., AIP Conf. Ser., First Stars and Galaxies: Challenges in the Next Decade. in press
Tominaga N., Umeda H., Nomoto K., 2007, ApJ, 660, 516
Umeda H., Nomoto K., 2002, ApJ, 565, 385
Umeda H., Nomoto K., 2003, Nat, 422, 871
Vladilo G., Centurión M., Bonifacio P., Howk J. C., 2001, ApJ, 557, 1007
Vogt S. S. et al., 1994, SPIE, 2198, 362
Wolfe A. M. Gawiser E., Prochaska J. X., 2005, ARA&A, 43, 861
Woosley S. E., Weaver T. A., 1995, ApJS, 101, 181

This paper has been typeset from a TEX/LATEX file prepared by the author.